Title: Soldering a gas diffusion layer to a stainless steel bipolar plate using metallic tin.

Authors: Katie McCay[a,b], Ole Edvard Kongstein[b], Anders Oedegaard[b], Alejandro Oyarce Barnett[b], Frode Seland[a]

a Norwegian University of Science and Technology (NTNU), Department of Materials Science and Engineering, Norway

b SINTEF Materials and Chemistry, Norway

Corresponding author: Katie McCay

Abstract

A novel investigation to decrease the interfacial contact resistance of stainless steel bipolar plates was performed. A thin layer of Sn was electrodeposited onto a bipolar plate and subsequently joined with a gas diffusion layer through hot-pressing at a temperature around the melting point of tin. This procedure was optimised, depositing 30 μm of Sn onto the stainless steel bipolar plate before hot-pressing at 230 ^{o}C and 0.5 bar for 20 minutes. A contact resistance of 5.45 mΩ cm^{2} at 140 N cm^{-2} was obtained, with low values maintained after exposure to both in-situ and ex-situ conditions. The in-situ testing in a fuel cell produced excellent results, with minor increases in contact resistance from 8.8 to 9.2 mΩ cm^{2} and decreases in cell voltage from 0.714 to 0.667 V after 200 hours of operation. These values are comparable to gold plated stainless steel, showing that combining a gas diffusion layer with electrodeposited Sn through hot-pressing is a promising low-cost coating for bipolar plates in PEM fuel cells.

Keywords

PEM Fuel Cell

Stainless Steel Bipolar Plate

Electrodeposition

Tin

Interfacial Contact Resistance

1. Introduction

In recent years, a greater demand for substitutes to fossil fuels has prompted the development of Proton Exchange Membrane (PEM) Fuel Cells. PEMFCs represent highly efficient energy conversion devices that are a viable alternative to combustion engines in the automobile industry [1]. Large car manufacturing companies, such as Toyota, Honda and Hyundai have set up long term plans to develop and introduce fuel cell technology for this industry [2–4]. However, a number of challenges have to be overcome before such electrochemical energy conversion devices are economically and practically feasible for mass implementation, including intrinsic limitations concerning durability, longevity and costs.

Numerous studies have looked into development of improved catalysts [5–7], ion conducting membranes [8–10] and catalytic layers [11–13] for optimised performance. Over the last few decades, more attention has been devoted to the bipolar plate (BPP) which is estimated to contribute 11-45 % of the overall fuel cell cost and 45-80 % of the stack weight [14–17]. BPPs must allow even distribution and separation of the anode and cathode feeds, facilitate removal of the waste products, manage heat produced during operation, and provide mechanical support for the stack as well as the membrane electrode assemblies (MEA) [17,18]. Due to their numerous tasks within the cell, the BPP must meet a strict series of criteria. The plates must be lightweight yet mechanically supportive to minimize overall weight, have high electrical conductivity and low interfacial contact resistance to both anode and cathode to minimise ohmic losses [19]. They must also be thermally conductive to remove excess heat, have high corrosion resistance to be long lasting and avoid contamination of catalyst and electrolyte as well as being impermeable to the reactant gases to minimise fuel crossover [20].

Consequently, a vast number of different BPP materials have been investigated [21–24]. Due to the inherent limitations of graphite [25] and other carbon based BPPs [17], metal plates are now considered the most promising candidates, with stainless steel found to be more suitable than titanium [26], nickel [27] or aluminium [28] alloy plates. Stainless steels have a significantly lower manufacturing cost and a higher strength than graphite [29], as well as a high electrical conductivity and low gas permeability. The main drawback of a metallic BPP is its struggle to maintain both low contact resistance and high corrosion resistance inside the fuel cell environment. When undergoing corrosion processes, the stainless steel releases metal ions that could lead to poisoning of the membrane and catalyst [17]. Another issue is the non-conductive oxide layer (e.g. chromium oxide, Cr_2O_3) that forms on the surface of the stainless steel upon contact with air and water, increasing contact resistance [30]. In order to limit the formation of such oxides and ions, a series of protective coatings have been developed for the stainless steel BPPs. A large amount of research has been done into different coating materials, including carbon based coatings [31–33], metal nitrides [34–36], carbides [37–39] and noble metals [40,41], many of which have improved the corrosion resistance and the Interfacial Contact Resistance (ICR) of the BPP to the standards set by the US Department

of Energy [42]. However, the coating methods for many of these BPPs, such as physical vapour deposition (PVD) or plasma nitriding, are costly, so a cheaper alternative must be found if stainless steel bipolar plates are to become commercially viable.

Tin is widely used as a solder in the electronics industry due to its high electrical conductivity, good wettability, low cost and reliability [43,44]. It is also easy to produce a well-defined layer of Sn by electrodeposition onto a metallic substrate, a technique that is popular due to its low cost, simplicity and good controllability of coating morphology and thickness [45,46]. As similar criteria need to be met for fuel cell applications, electrodeposition can be considered a good candidate for further research.

Tin has also been proven to improve the corrosion properties of stainless steels through the formation of a dense SnO_2 passive layer, which inhibits further corrosion [47–49]. Despite this, Sn has been thought unsuitable for PEM applications due to the potential poisoning of the membrane and catalyst by Sn ions. This has proven not to be the case by Iwai et al., who reported no decomposition of nafion membranes when exposed to Sn [50], in fact, the proton conductivity and Young's modulus of nafion membranes is improved upon small additions of Sn [51]. It has been reported that SnO_2 modified membranes have improved durability, reduced release of F^- ions and retained a higher Pt loading through the cell lifetime [52,53]. Sn based catalysts have also been used extensively for methanol oxidation with promoting effects [54–56], indicating that Sn has no negative impact on the catalyst or membrane during operation.

In this work we cover stainless steel bipolar plates with a thin and uniform layer of electroplated Sn in order to exploit the high electrical conductivity as well as the high corrosion resistance offered by metallic Sn and Sn oxide, respectively. The novel idea in this work is to join (solder) the tin-plated stainless steel bipolar plate with a pre-cut gas diffusion layer (GDL) through hot pressing at a temperature around the melting point of tin. This process softens the Sn coating, and the addition of mechanical pressure forces it into the pores of the GDL where it cools and solidifies, soldering the materials together as demonstrated in Figure 1. This should produce improved through-plane electrical and thermal conductivity, yielding extremely low contact resistances.

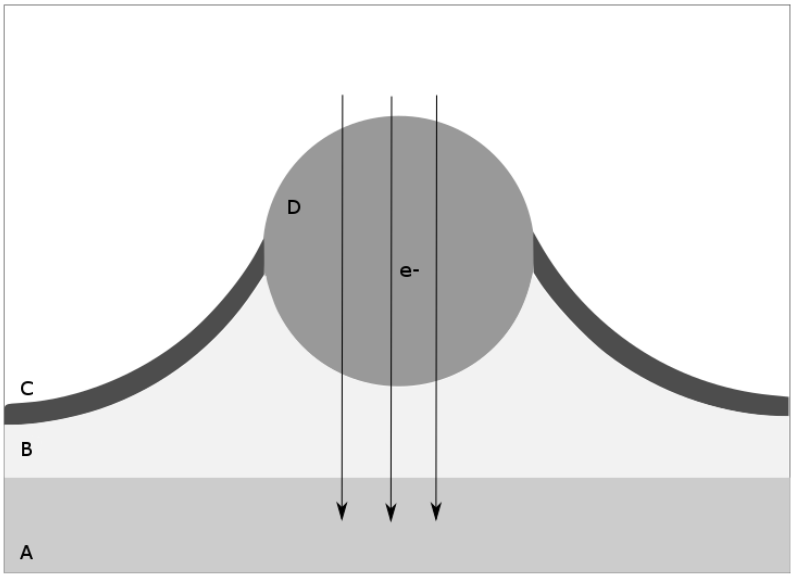

Figure 1. The combined Sn/GDL concept. A is the steel bipolar plate, B the deposited Sn, C the SnO_2 layer and D the carbon fibre from the GDL. Electrons can move through the system without obstruction whilst the SnO_2 prevents further oxidation of Sn.

The BPP will be exposed to operating PEM conditions, including a slightly acidic environment and voltages up to 1.4 V_{SHE}, that may occur during start up and shut down [57]. During exposure, the outer layer of the deposited Sn will oxidise to form a passive SnO_2 layer [58], as indicated by the Pourbaix diagram [59]. This layer remains conductive and protects the underlying Sn and stainless steel substrate from further oxidation, whilst maintaining a good conductivity and low contact resistance.

The preparation procedure and quality of the joined BPP/GDL material are studied with respect to conductivity and durability through a series of measurements, including interfacial contact resistance (ICR), ex-situ chronoamperometry and electron microscope imaging with elemental analysis. Finally, long-term in-situ testing in a simulated fuel cell environment is performed. The produced plates show good adhesion and low contact resistance, even after being exposed to a simulated fuel cell environment. Thus, the method described in this work brings a move towards simple, yet reliable, coating methods for BPPs in PEM systems.

2. Experimental

AISI 316L bipolar plates were used as received from Elring Klinger for all tests. The total surface area of the plates was 39.2 cm^2, with a land area of 6.2 cm^2 for ICR measurements. Potentiostatic and ICR measurements were recorded ex-situ, as well as Scanning Electron Microscopy (SEM) and Energy Dispersive Spectroscopy

(EDS) analysis using a Hitatchi S-3400N. In-situ fuel cell testing of the plates was performed using a Greenlight G-40 Fuel Cell Test Station equipped with a Gamry Reference 3000 Potentiostat.

2.1 Construction of combined Bipolar Plate with GDL

Prior to all experimental work, the stamped SS316L BPP was etched in HCl (12.8 wt.%, 3.5 M, room temperature, 15 minutes) to remove any oxide layer, followed by rinsing in deionised water and drying under nitrogen at room temperature. A coating of peel-able Micro super XP 2000 stop-off lacquer was then applied to the backside of the BPP with a paintbrush.

The electroplating solution was prepared as follows: Tin(II) sulfate (36.17 g, purity ≥ 95%, Sigma Aldrich) was dissolved in 700 mL deionized water (Milli-Q Integral pure water system). Sulphuric acid (98 %, 100 ml, Sigma Aldrich) was added dropwise, and left to cool. SLOTOTIN 71™ (Schlötter, 20 ml) starter and SLOTOTIN 72™ (Schlötter, 3 ml) brightener were added to the solution, which was then diluted with deionized water to a total volume of 1.0 L. The stainless steel bipolar plate was immersed in the electroplating bath and connected to the negative pole of the current source. A pair of Sn electrodes were used as the counter electrode (positive pole) and a current density of 1.5 A dm^{-3} was applied to obtain a deposition rate of 0.7 µm min^{-1} assuming 100 % current efficiency.

After removal of the plate from the solution, it was cleaned with deionized water and the lacquer peeled from the back side. Immediately after, the cleaned plate was placed on top of a pre-cut GDL (H23C6 GDL, Freudenberg FFCT) [60], and hot-pressed at a set pressure, temperature and time before cooling to room temperature either slowly under applied pressure or rapidly at atmospheric pressure. This process was repeated for three identical plates to obtain a standard deviation.

2.2. Interfacial Contact Resistance (ICR) Measurements

ICR measurements were performed before and after each corrosion test using a setup adapted from Wang et al. [61] and identical to the one used in [62]. The sample was placed between two gold-coated copper conducting plates, and a current of 2 A was passed between the bottom plate and the top plate. The

voltage between a spring-loaded gold pin and the top plate, through the sample, was recorded as the compaction force was increased from 70 to 650 N cm^{-2}. All quoted values for ICR are recorded at 140 N cm^{-2}, which is the standard in-situ compaction pressure [61]. It was assumed that the bulk resistance of the gold and copper plates, as well as the bulk resistance of the SS316L BPP and GDL were negligible.

2.3 Ex-situ Corrosion Testing

The bipolar plate specimens were evaluated for their corrosion characteristics through potentiostatic measurements using a Gamry Ref 600 potentiostat. The combined BPP/GDL functioned as the working electrode, and was submerged in a Na_2SO_4 (0.1M) /H_2SO_4 mixture adjusted to pH 5.5. A Pt mesh was used as the counter electrode. Prior to potentiostatic testing, electrolyte was injected into the channels of the bipolar plate with a syringe. A mercury-mercurous sulfate reference electrode ($Hg/Hg_2SO_4/K_2SO_{4Sat}$, 0.64 V_{SHE}) was connected to the working electrolyte compartment via a salt bridge. The electrolyte was heated to 80 ^oC and purged with nitrogen prior to all testing. All potentials in this work are recalculated and expressed versus a standard hydrogen electrode unless stated otherwise. For potentiostatic measurements, the samples were first stabilised at open circuit potential before applying a voltage of 1.4 V_{SHE} for 1 hour.

2.4 In-situ Fuel Cell Testing

A fuel cell test station equipped with a cell of active area of 15 cm^2 was used. The MEA was a GORE® PRIMEA® MEA of thickness 15 µm, Pt content of 0.1 mg cm^{-2} at the anode and 0.4 mg cm^{-2} at the cathode. H23C6 GDL (Freudenberg FFCT) [60] was used throughout this study.

The fuel cell was constructed with two of the combined BPP and GDL plates, one placed on each side of a membrane electrode assembly (MEA) with the back side of the steel bipolar plates in direct contact with gold current collectors, and then clamped together. The clamping pressure was piston-regulated and separated from the sealing pressure at 200 kPa over the area of the bipolar plate, equivalent to 140 N cm^{-2}. The cell was operated at 70 ^oC, with synthetic air supplied in excess at the cathode (AGA 99.999 %, stoichiometry 5) and

hydrogen in excess at the anode (AGA 99.999 %, stoichiometry 3). The excess of gas ensured a stable performance and minimum variation in reactant concentration throughout the entire length of the bipolar plate. Backpressures of 20 kPa and 30 kPa were applied to the anode and cathode, respectively.

The catalytic layers and membrane interactions were activated for 1 hour in fully humidified N_2, 70°C, at both the anode and cathode, followed by cycling for 3 hours between 0.7 V and 0.5 V under H_2/air.

A cycling procedure of high and low current densities (1.2 and 0.5 A cm^{-2}), interspaced with shut-downs and start-ups, as seen in Figure 2, was performed for 170 hours.

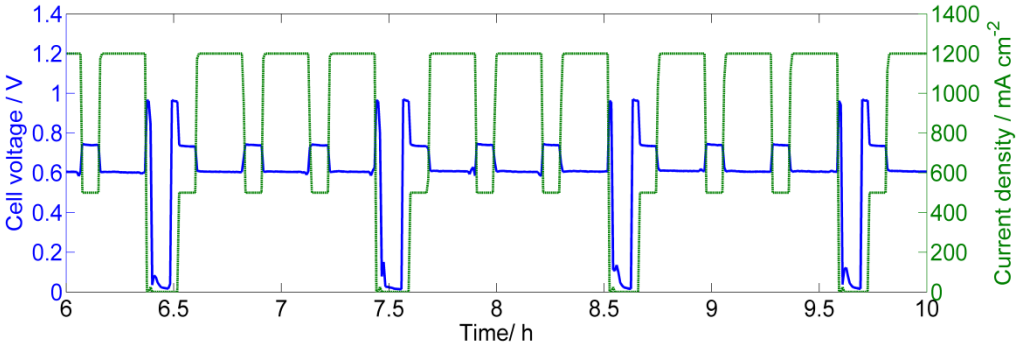

Figure 2 The cycling procedure during in-situ testing

After completion of the initial 170 hours test procedure, the cell was shut-down and purged with nitrogen overnight before the test was resumed until a total of 200 hours of testing was complete.

Over the course of the in-situ testing, impedance measurements were recorded during high current density operation, over a frequency range of 10 kHz to 100 mHz. The real value of the impedance recorded at 1 kHz was used as the high frequency resistance (HFR), and assumed to represent the ohmic resistance in the circuit. Cyclic voltammetry of the fuel cell was conducted with H_2 on the anode and N_2 on the cathode to provide an estimate of the change in the electrochemical active surface (ECSA) area at the cathode.

The same procedure was implemented for two control plates, gold coated SS316L and TiN+C coated SS316L, both provided by Elring Klinger.

3. Results & Discussion

3.1 Optimisation of procedure: Combining BPP and GDL with Sn

The procedure for combining the metallic plate with the GDL through Sn impregnation via hot pressing was optimized firstly with respect to lowest possible ICR and then to highest corrosion resistance. The effects on interfacial contact resistance and corrosion rate of various preparation parameters such as hot press pressure, temperature and time, as well as deposition charge (coating thickness) and cooling method, were investigated. Before the Sn/GDL plates could be tested in-situ, each of these parameters was optimised to increase performance.

3.1.1 Hot Pressing

When hot pressing, the pressure was set at 140 N cm^{-2}, equivalent to the in-situ pressure. Increasing the pressure could cause flattening of the BPP channels, compromising the structure. Blocking of the channels by the GDL could also occur, reducing the cell performance by hindering the transport of reactants into and waste products out of the cell. Lower pressures reduce adhesion between the GDL and BPP as permeation of the Sn into the GDL is lessened, reducing the length of the conduction pathway and the conductivity.

When optimising the hot pressing temperature, those around the melting point of Sn (231.9 ^{o}C [63]) were selected to investigate how the degree of melting of Sn could produce a best possible electronic contact between the metallic plate and the carbon based GDL. Table 1 shows the ICR values recorded after pressing at temperatures between 226 and 232 ^{o}C. At temperatures above 230 ^{o}C, the Sn becomes ductile enough to penetrate the GDL more effectively, ensuring an increased contact area and a better pathway for current, lowering the average ICR from 8.0 mΩ cm^2 at 228 ^{o}C down to 5.4 mΩ cm^2 at 230 ^{o}C. In addition to an improved through-plane electronic conductivity, the plates prepared with a hot press temperature of 230 ^{o}C offered an improved adhesion due to the infiltration of GDL fibres into the tin, something that did not occur at temperatures lower than 230 ^{o}C. Raising the temperature even further causes the Sn to run into the channels. For this reason, a temperature of 230 ^{o}C was used for all further plates.

Table 1. Contact resistance (mΩ cm^2) at various hot press times and temperatures

Press Temp (°C)	226	228	230	232
Press time (min)				
1	7.9	6.5	6.6	5.4
10	8.3	8.4	5.4	7.6
60	6.0	9.2	4.4	5.6

The time required for hot pressing was also investigated. Varying the hot-press time from 1 to 60 minutes produced variations in contact resistance with no clear pattern, as seen in Table 1. 20 minutes was found to be a suitable duration to allow the Sn to reach the desired temperature.

3.1.2 Cooling Method

The effect on ICR of cooling the samples using two different methods was investigated (Figure 3). The ICRs for both cooling rapidly under atmospheric pressure (fast cool) or slowly under applied pressure (slow cool) were comparable before corrosion, at 6.8 and 7.1 mΩ cm^2 at 140 N cm^{-2}. After polarisation to 1.4 V for 1 hour, a significantly improved ICR was observed for the slowly cooled plate, 13.2 compared to 17.9 mΩ cm^2 at 140 N cm^{-2}. The slow cooling is suggested to result in increased grain sizes and fewer grain boundaries and therefore fewer active sites for corrosion [64]. In addition, leaving the sample under continuous pressure when being cooled forces the Sn to stay in contact with the GDL whilst solidifying.

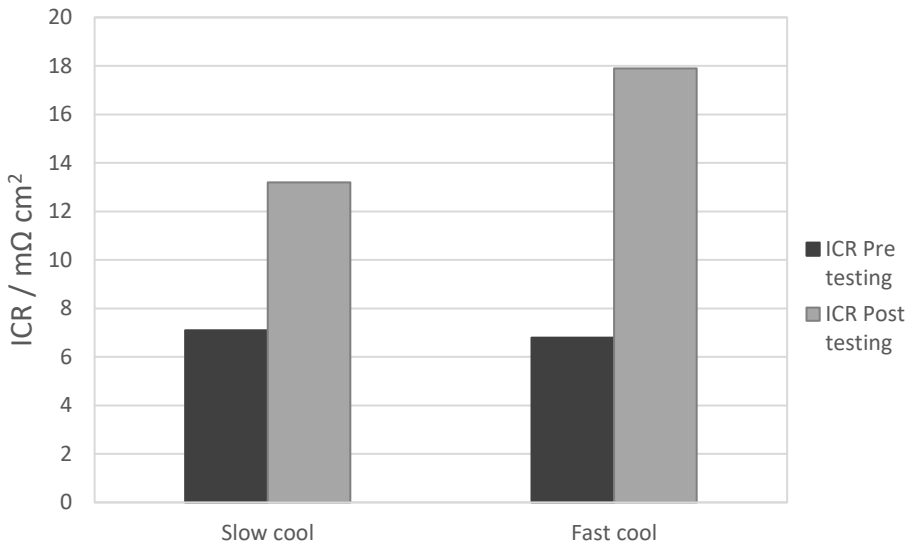

Figure 3 Comparison of the quickly vs slowly cooled plates before and after corrosion testing

This shows the importance of precise control of processing parameters. The slower cooling procedure was used in the production of all further plates.

3.1.3 Thickness of Sn Layer

It is important that the Sn layer is thick enough to allow the Sn to permeate into the GDL and form a good contact. ICR measurements before and after corrosion testing were done for a series of Sn thicknesses from 10 to 60 µm (Figure 4).

Before corrosion testing, all ICR values were lower than DoE requirements, and decreased with an increasing tin-plating thickness, most likely due to greater permeation of the Sn into the GDL and increased electrical contact between the layers. In addition, the bulk resistance of Sn is low (1.09 $x10^{-7}$ Ω m [65]), so a thicker layer does not impact negatively on the conductivity. In fact, the contact resistance measured initially was lower than values obtained from gold and cleaned stainless steel plates using the same equipment. This is a clear indication that hot-pressing the tin-plated BPP with the GDL produces a better conduction pathway than simply placing the GDL on top of the BPP.

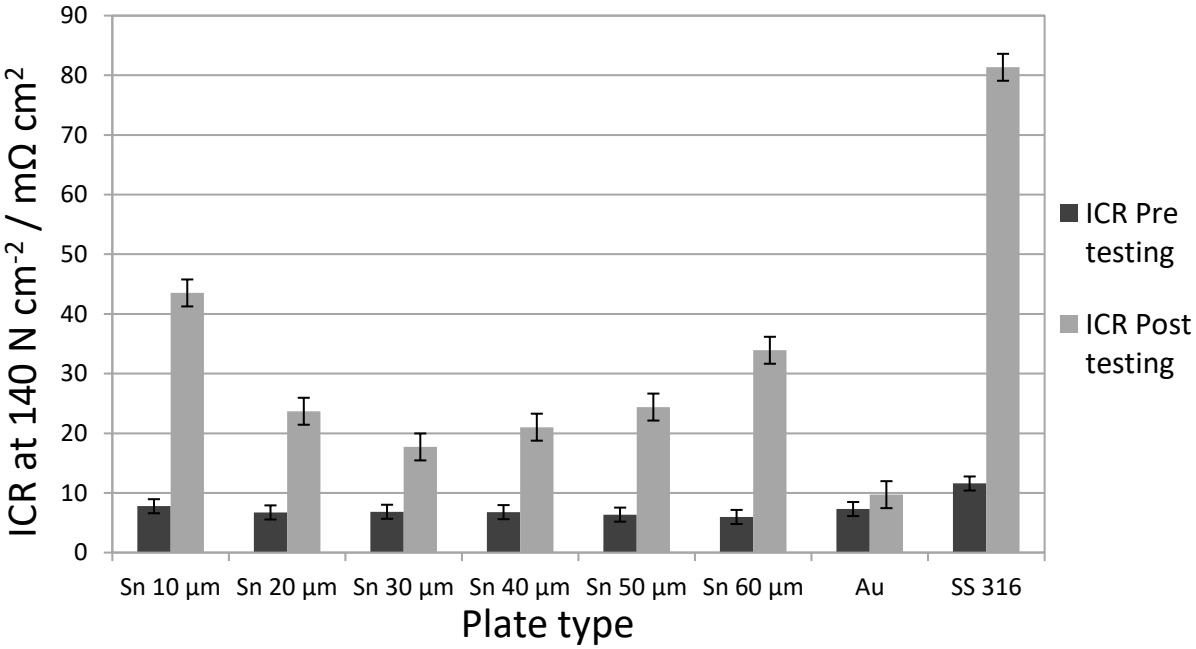

Figure 4 Comparison of coating thickness against ICR before and after ex-situ testing

After potentiostatic testing for 1 hour at 1.4 V, the ICR of the samples increased vastly, up to 560 % for the thinner coatings. The significant increase in through-plane resistivity must be due to detrimental oxidation processes occurring during the high potential operation. Figure 5 shows cross-sectional EDS images for the series of tin-plating thicknesses after corrosion testing. It is clear that the corrosion testing led to a significant removal of tin. In fact, the deposited Sn layer (green colour) in Figure 5 A (10 µm) was reduced from a thickness of 10 µm to being non-existent. Furthermore, the GDL (red colour) is also not present in Figure 5 A. The removal of Sn during corrosion testing reduced adhesion between the GDL and BPP enough that the GDL entirely delaminated from the plate. From Figure 5 B (20 µm), there is also very little of the Sn layer remaining, but just enough to continue to adhere the GDL to the BPP. The Sn is oxidised to SnO_2 during the corrosion testing, but instead of providing corrosion protection to the underlying Sn bulk deposit it delaminates and falls off the plate into the electrolyte.

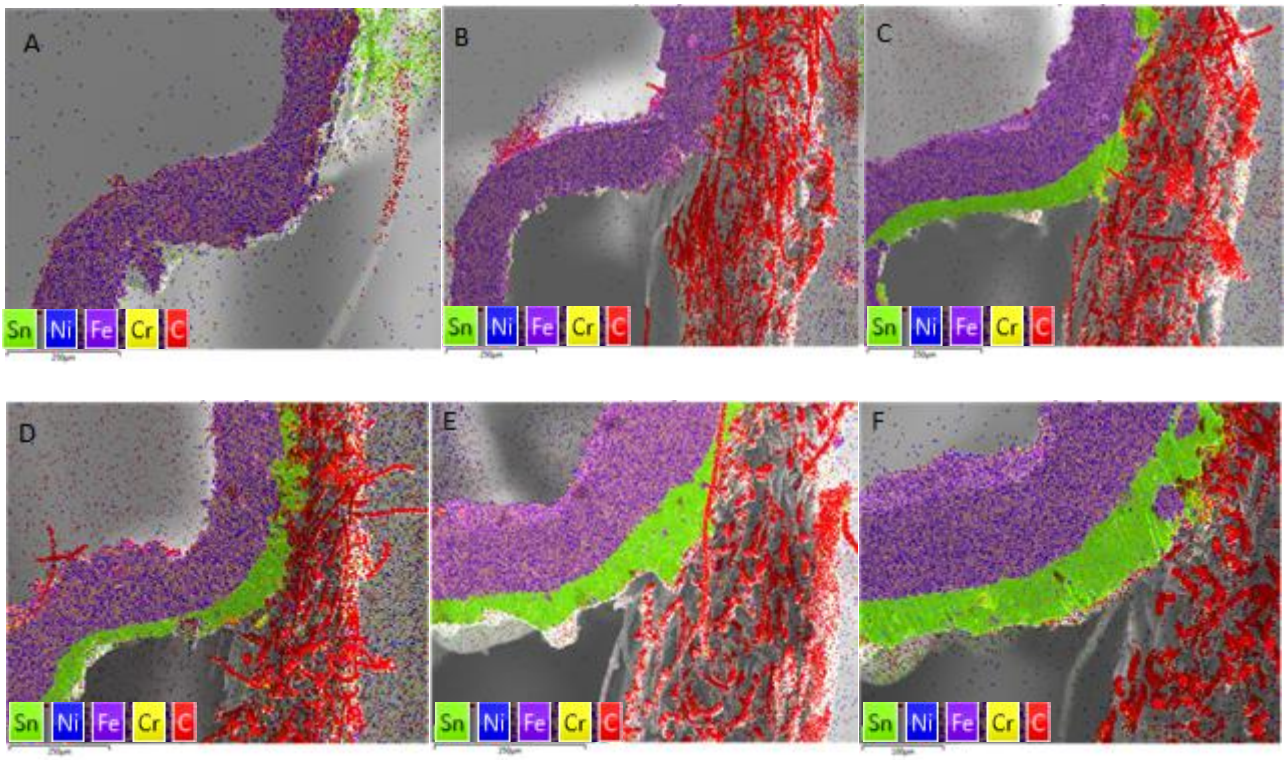

Figure 5. Cross-sectional EDS images of BPPs & GDL with varying thickness of Sn after ex-situ testing, purple representing the bipolar plate, green the Sn and red the GDL. The initial thickness of deposits was 10, 20, 30, 40, 50 and 60 µm on figure A to F respectively.

As the thickness of the Sn layer increases, in Figure 5 C, D, E and F, there is more Sn left after corrosion and consequently greater adhesion. Interestingly, the ICR of the thickest coatings, 50 and 60 µm, also increased by a large amount, up to 570 %, after polarization to 1.4 V for 1 h. This is possibly due to the larger volume of SnO_2 formed during the corrosion process. SnO_2 has a lower conductivity than metallic Sn[63], contributing to the observed increase in ICR. Additionally, the SnO_2 produced after testing has a larger volume than Sn, so falls off the surface of the Sn and causes delamination between the remaining Sn layer and the GDL. This excess SnO_2 is not visible in the EDS images, as it is removed during the corrosion testing, as observed by a milky white suspension in the electrolyte.

From Figure 4, the best performing bipolar plate was found to have a Sn layer thickness of around 30 µm, which was then used for all subsequent plates. As seen in the images in Figure 5 (C and D), it is obvious that the Sn has permeated into the GDL during the hot-pressing stage, so despite the loss of Sn that took place during the high voltage procedure, there is still a good conduction pathway and the ICR remains low. The ICR increased by around 260 % after corrosion testing. Despite this being less than for the other thicknesses, all

of which showed better performance than bare SS316L, there is still a necessity to improve the deposition process or stabilise the SnO_2 layer that is formed after exposure to the PEM environment.

3.2 In-situ Analysis

An in-situ study of the optimised Sn/GDL BPP was performed and compared to identical tests on Au and TiN+C coated SS316L BPPs. Both before and after the 200 h cycling procedure, a full series of standard measurements including electrochemical active surface area (ECSA), H-crossover and high frequency resistance (HFR) were undertaken to ensure normal operation of the cell.

Some differences in performance were observed at the beginning of life, as seen in Figure 6. The HFR for the Sn/GDL plate is higher than for the other two plates, and the cell voltage is lower, 0.630 V at 1 A cm^{-2} compared to 0.639 V and 0.645 V for Au and TiN+C, respectively. These differences arise from differing resistances within the cell, which include all ohmic losses: membrane resistance, electronic resistances and all contact resistances.

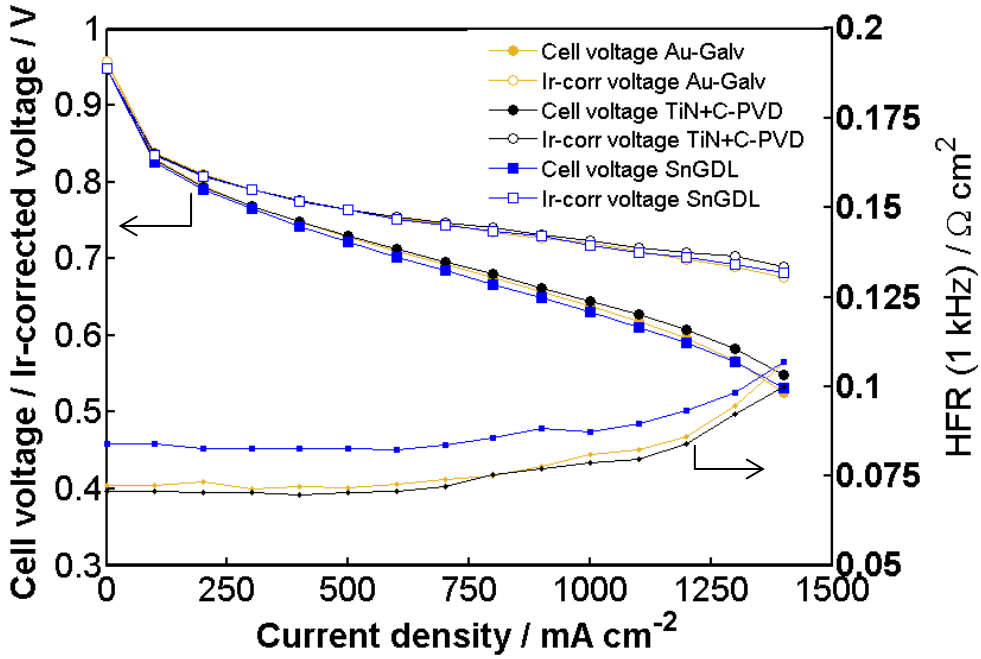

Figure 6. Beginning of life performance of the fuel cell equipped with Au (yellow) TiN+C (black) and Sn/GDL (blue) bipolar plates.

During cycling, the cell voltage and HFR were monitored. A visible drop in cell voltage and an increase in HFR, as seen in Figure 7, occurs for all plates due to the degradation of the membrane and a reduction in ECSA. The Sn/GDL bipolar plate is degrading at a slower rate than the other bipolar plates, despite its initially poorer performance. After 170 hours of cycling, all plates show similar cell voltages. Moreover, after the shut down and a further 30 hours of operation, the Sn/GDL and TiN+C plates outperform the Au standards, with a higher cell voltage maintained after a total of 200 hours of operation.

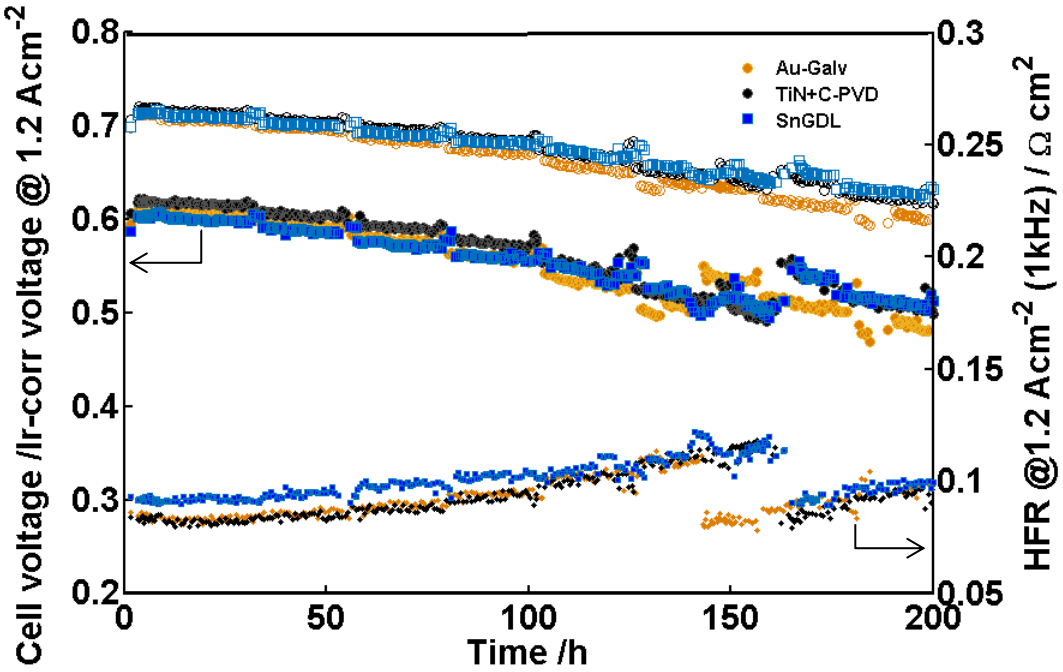

Figure 7. 200 hours in-situ cell voltage and high frequency resistance performance of a PEM fuel cell equipped with Au (yellow circles), TiN+C (black circles) and Sn/GDL (blue squares) BPPs.

There are no indications that any formation of SnO_2 on the Sn/GDL plate is affecting performance, as was the case during potentiostatic ex-situ testing. Cyclic voltammetry confirmed that there is no adsorption of Sn onto the catalyst, and although a decrease in catalytic surface area was observed, this is consistent with the control plates, indicating no negative effect of Sn on the catalyst. Nor is the Sn affecting the membrane performance as the HFR after 200 h is equal for all plates (Figure 7).

Comparing the voltage performance, the BPP that ended up with the smallest total drop in cell voltage was the Sn/GDL BPP, with a drop from 0.714 to 0.667, indicating that it would have the longest lifetime in the cell. More long term testing is needed to confirm this.

After testing for 200 hours, the plates were removed from the cell and their ICR was tested ex-situ, as seen in Table 2.

Table 2 Ex-situ interfacial contact resistance measurements before and after in-situ testing

Plate	ICR before (mOhm cm^2)	ICR after - Anode (mOhm cm^2)	ICR after - Cathode (mOhm cm^2)
Au	7.7	7.2	7.4
TiN+C	8.4	9.3	10.3
Sn/GDL	8.8	9.2	19.7

The Sn/GDL combined plate performed well when compared with the control plates, with a very small increase in ICR being observed at the anode side. However, a significant increase was observed on the cathode side of the cell. As no corresponding sharp increase in HFR was observed in-situ, the increase observed during the ex-situ ICR could be due to post-mortem disassembly of the cell, during which the GDL may slightly delaminate from the Sn-coated BPP.

4. Conclusions

A novel bipolar plate concept that significantly diminishes the interfacial contact resistance with the gas diffusion layer was successfully demonstrated. An optimised electrodeposition process was developed to produce a combined Sn/GDL protective layer on an SS316L bipolar plate. Very low ICR values were obtained before ex-situ corrosion testing, due to the uninhibited conduction pathways connecting the GDL and BPP through the soldered tin. If maintained in-situ, these pathways will provide easy conduction through the lifetime of the cell. However, the ICR increased after corrosion testing due to the instability of SnO_2 on the surface of the coating leading to the breakdown of the conduction pathways.

The optimised conditions for the deposition of Sn onto the SS316L BPP are as follows: A plating thickness of 30 µm was deposited onto the pre-cleaned BPP, before hot pressing with a pre-cut GDL at 230 ^{o}C for 20 minutes at a pressure of 0.5 bar, and cooling slowly to room temperature. This procedure obtained the lowest contact resistance of 6.5 mΩ cm^2 at 140 Ncm^{-2}, well below U.S DoE targets, and was tested both ex-situ and in-situ. The contact resistance increased to 13.2 mΩ cm^2 at 140 Ncm^{-2} after ex-situ testing in Na_2SO_4 at pH 5.5 and 80 ^{o}C, with 1.4 V_{SHE} applied for 1 h. In-situ testing produced results equivalent to high-cost PVD coatings, with interfacial contact resistance values increasing from 8.8 to 9.2 mΩ cm^2 on the anode side and 19.7 mΩ cm^2 on the cathode side, and the cell voltage decreasing from 0.714 to 0.667 V over the course of 200 hours. No degradation of the catalyst or membrane caused by the release of Sn ions from the bipolar plate was observed after 200 hours.

Future work must focus on enhancing the stability of the SnO_2 oxide layer, and introducing alloying elements to improve long-term performance.

Acknowledgements

The research leading to these results has received funding from the European Union's Seventh Framework Programme (FP7/2007-2013) for the Fuel Cells and Hydrogen Joint Technology Initiative under grant agreement number 303449 10.

KM thanks the Department of Materials Science and Engineering at NTNU for the award of a scholarship.

References

[1] Wang Y, Chen KS, Mishler J, Cho SC, Adroher XC. A review of polymer electrolyte membrane fuel cells: Technology, applications, and needs on fundamental research. Appl Energy 2011;88:981–1007. doi:10.1016/j.apenergy.2010.09.030.

[2] Barrett S. Fuel cells power forward on the roads and for power generation. Renew Energy Focus 2017;18:29–32. doi:10.1016/J.REF.2017.03.002.

[3] Samuelsen S. The automotive future belongs to fuel cells range, adaptability, and

refueling time will ultimately put hydrogen fuel cells ahead of batteries. IEEE Spectr 2017;54:38–43. doi:10.1109/MSPEC.2017.7833504.

[4] Kojima K, Fukazawa K. Current Status and Future Outlook of Fuel Cell Vehicle Development in Toyota. ECS Trans 2015;69:213–9. doi:10.1149/06917.0213ecst.

[5] Zhang S, Yuan X-Z, Hin JNC, Wang H, Friedrich KA, Schulze M. A review of platinum-based catalyst layer degradation in proton exchange membrane fuel cells. J Power Sources 2009;194:588–600. doi:10.1016/j.jpowsour.2009.06.073.

[6] Shao Y, Sui J, Yin G, Gao Y. Nitrogen-doped carbon nanostructures and their composites as catalytic materials for proton exchange membrane fuel cell. Appl Catal B Environ 2008;79:89–99. doi:10.1016/j.apcatb.2007.09.047.

[7] Dai L, Xue Y, Qu L, Choi H-J, Baek J-B. Metal-Free Catalysts for Oxygen Reduction Reaction. Chem Rev 2015;115:4823–92. doi:10.1021/cr5003563.

[8] Kreuer K-D. Ion Conducting Membranes for Fuel Cells and other Electrochemical Devices. Chem Mater 2013;26:361–80. doi:10.1021/cm402742u.

[9] Smitha B, Sridhar S, Khan AA. Solid polymer electrolyte membranes for fuel cell applications - A review. J Memb Sci 2005;259:10–26. doi:10.1016/j.memsci.2005.01.035.

[10] Peighambardoust SJ, Rowshanzamir S, Amjadi M. Review of the proton exchange membranes for fuel cell applications. Int J Hydrogen Energy 2010;35:9349–84.

[11] Banham D, Ye S. Current Status and Future Development of Catalyst Materials and Catalyst Layers for Proton Exchange Membrane Fuel Cells: An Industrial Perspective. ACS Energy Lett 2017;2:629–38.

doi:10.1021/acsenergylett.6b00644.

[12] Shao Y, Liu J, Wang Y, Lin Y. Novel catalyst support materials for PEM fuel cells: current status and future prospects. J Mater Chem 2009;19:46–59. doi:10.1039/b808370c.

[13] Zhang J. PEM fuel cell electrocatalysts and catalyst layers: Fundamentals and applications. 2008. doi:10.1007/978-1-84800-936-3.

[14] Wang H, Turner JA. Reviewing Metallic PEMFC Bipolar Plates. Fuel Cells 2010;10:510–9. doi:10.1002/fuce.200900187.

[15] Yuan XZ, Wang HJ, Zhang JJ, Wilkinson DP. Bipolar plates for PEM fuel cells - From materials to processing. J New Mater Electrochem Syst 2005;8:257–67.

[16] Mehta V, Cooper JS. Review and analysis of PEM fuel cell design and manufacturing. J Power Sources 2003;114:32–53. doi:10.1016/S0378-7753(02)00542-6.

[17] Antunes RA, Oliveira MCL, Ett G, Ett V. Corrosion of metal bipolar plates for PEM fuel cells: A review. Int J Hydrogen Energy 2010;35:3632–47. doi:10.1016/j.ijhydene.2010.01.059.

[18] Peng L, Yi P, Lai X. Design and manufacturing of stainless steel bipolar plates for proton exchange membrane fuel cells. Int J Hydrogen Energy 2014;39:21127–53. doi:10.1016/j.ijhydene.2014.08.113.

[19] Netwall CJ, Gould BD, Rodgers JA, Nasello NJ, Swider-Lyons KE. Decreasing contact resistance in proton-exchange membrane fuel cells with metal bipolar plates. J Power Sources 2013;227:137–44. doi:10.1016/j.jpowsour.2012.11.012.

[20] Zhang JJ, Zhang H, Wu JJ, Zhang JJ, Zhang H. PEM Fuel Cell Testing and Diagnosis.

2013. doi:10.1016/B978-0-444-53688-4.00007-3.

[21] Tawfik H, Hung Y, Mahajan D. Metal bipolar plates for PEM fuel cell-A review. J Power Sources 2007;163:755–67. doi:10.1016/j.jpowsour.2006.09.088.

[22] Taherian R. A review of composite and metallic bipolar plates in proton exchange membrane fuel cell: Materials, fabrication, and material selection. J Power Sources 2014;265. doi:10.1016/j.jpowsour.2014.04.081.

[23] Asri NF, Husaini T, Sulong AB, Majlan EH, Daud WRW. Coating of stainless steel and titanium bipolar plates for anticorrosion in PEMFC: A review. Int J Hydrogen Energy 2016. doi:10.1016/j.ijhydene.2016.06.241.

[24] Hermann A, Chaudhuri T, Spagnol P. Bipolar plates for PEM fuel cells: A review. Int. J. Hydrogen Energy, vol. 30, 2005, p. 1297–302. doi:10.1016/j.ijhydene.2005.04.016.

[25] Kakati BK, Ghosh A, Verma A. Efficient composite bipolar plate reinforced with carbon fiber and graphene for proton exchange membrane fuel cell. Int J Hydrogen Energy 2013;38:9362–9. doi:10.1016/j.ijhydene.2012.11.075.

[26] Wang SH, Peng J, Lui WB. Surface modification and development of titanium bipolar plates for PEM fuel cells. J Power Sources 2006;160:485–9. doi:10.1016/j.jpowsour.2006.01.020.

[27] Brady MP, Wang H, Yang B, Turner JA, Bordignon M, Molins R, et al. Growth of Cr-Nitrides on commercial Ni-Cr and Fe-Cr base alloys to protect PEMFC bipolar plates. Int J Hydrogen Energy 2007;32:3778–88. doi:10.1016/j.ijhydene.2006.08.044.

[28] Mawdsley JR, Carter JD, Wang X, Niyogi S, Fan CQ, Koc R, et al. Composite-coated

aluminum bipolar plates for PEM fuel cells. J Power Sources 2013;231:106–12. doi:10.1016/j.jpowsour.2012.12.074.

[29] Sun H, Cooke K, Eitzinger G, Hamilton P, Pollet B. Development of PVD coatings for PEMFC metallic bipolar plates. Thin Solid Films, 2013. doi:10.1016/j.tsf.2012.10.094.

[30] Lædre S, Kongstein OE, Oedegaard A, Seland F, Karoliussen H. The effect of pH and halides on the corrosion process of stainless steel bipolar plates for proton exchange membrane fuel cells. Int J Hydrogen Energy 2012;37:18537–46. doi:10.1016/j.ijhydene.2012.09.021.

[31] Chung CY, Chen SK, Chin TS, Ko TH, Lin SW, Chang WM, et al. Catalyst layer-free carbon-coated steel-An easy route to bipolar plates of polymer electrolyte membrane fuel cells: Characterization on structure and electrochemistry. J Power Sources 2009;186:393–8. doi:10.1016/j.jpowsour.2008.10.047.

[32] Jin W, Feng K, Li Z, Cai X, Yu L, Zhou D, et al. Properties of carbon film deposited on stainless steel by close field unbalanced magnetron sputter ion plating. Thin Solid Films 2013;531:320–7. doi:10.1016/j.tsf.2013.01.036.

[33] Husby H, Kongstein OE, Oedegaard A, Seland F. Carbon-polymer composite coatings for PEM fuel cell bipolar plates. Int J Hydrogen Energy 2014;39:951–7. doi:10.1016/j.ijhydene.2013.10.115.

[34] Turan C, Cora ??mer Necati, Ko?? M. Contact resistance characteristics of coated metallic bipolar plates for PEM fuel cells - Investigations on the effect of manufacturing. Int J Hydrogen Energy 2012;37:18187–204. doi:10.1016/j.ijhydene.2012.09.042.

[35] Jin J, Zhu Z, Zheng D. Influence of Ti content on the corrosion properties and contact resistance of CrTiN coating in simulated proton exchange membrane fuel cells. Int J Hydrogen Energy 2017;42:11758–70. doi:10.1016/j.ijhydene.2017.02.014.

[36] Wang S, Hou M, Zhao Q, Jiang Y, Wang Z, Li H, et al. Ti/(Ti,Cr)N/CrN multilayer coated 316L stainless steel by arc ion plating as bipolar plates for proton exchange membrane fuel cells. J Energy Chem 2017;26:168–74. doi:10.1016/j.jechem.2016.09.004.

[37] Wang L, Sun J, Kang B, Li S, Ji S, Wen Z, et al. Electrochemical behaviour and surface conductivity of niobium carbide-modified austenitic stainless steel bipolar plate. J Power Sources 2014;246:775–82. doi:10.1016/j.jpowsour.2013.08.025.

[38] Zhao Y, Wei L, Yi P, Peng L. Influence of Cr-C film composition on electrical and corrosion properties of 316L stainless steel as bipolar plates for PEMFCs. Int J Hydrogen Energy 2016;41:1142–50. doi:10.1016/j.ijhydene.2015.10.047.

[39] Huang NB, Yu H, Xu LS, Zhan S, Sun M, Kirk DW. Corrosion kinetics of 316L stainless steel bipolar plate with chromiumcarbide coating in simulated PEMFC cathodic environment. Results Phys 2016;6:730–6. doi:10.1016/j.rinp.2016.10.002.

[40] Feng K, Li Z, Cai X, Chu PK. Silver implanted 316L stainless steel as bipolar plates in polymer electrolyte membrane fuel cells. Mater Chem Phys 2011;126:6–11. doi:10.1016/j.matchemphys.2010.11.029.

[41] Lin K, Li X, Dong H, Du S, Lu Y, Ji X, et al. Surface modification of 316 stainless

steel with platinum for the application of bipolar plates in high performance proton exchange membrane fuel cells. Int J Hydrogen Energy 2017;42:2338–48. doi:10.1016/j.ijhydene.2016.09.220.

[42] US Department of Energy office of energy energy efficiency and renewable energy U. US DOE Technical Targets for Polymer Electrolyte Membrane Fuel Cell Components 2017. https://energy.gov/eere/fuelcells/doe-technical-targets-polymer-electrolyte-membrane-fuel-cell-components (accessed August 10, 2017).

[43] Lau JH, Wong CP, Lee N-C, Lee S-WR. Electronics Manufacturing: With Lead-Free, Halogen-Free, and Conductive-Adhesive Materials. The McGraw-Hill Companies, Inc.; 2003.

[44] Chriašteľová J, Ožvold M. Properties of solders with low melting point. J Alloys Compd 2008;457:323–8. doi:10.1016/j.jallcom.2007.03.062.

[45] Melo RL, Casciano PNS, Correia AN, Lima-Neto P de. Characterisation of electrodeposited and heat-treated Ni–Mo–P coatings. J Braz Chem Soc 2012;23:328–34. doi:10.1590/S0103-50532012000200020.

[46] Zhu XB, Cai C, Zheng GQ, Zhang Z, Li JF. Electrodeposition and corrosion behavior of nanostructured Ni-TiN composite films. Trans Nonferrous Met Soc China (English Ed 2011;21:2216–24. doi:10.1016/S1003-6326(11)60998-9.

[47] Pardo A, Merino MC, Carboneras M, Coy AE, Arrabal R. Pitting corrosion behaviour of austenitic stainless steels with Cu and Sn additions. Corros Sci 2007;49:510–25. doi:10.1016/j.corsci.2006.06.004.

[48] Pardo A, Merino MC, Carboneras M, Viejo F, Arrabal R, Muñoz J. Influence of Cu

and Sn content in the corrosion of AISI 304 and 316 stainless steels in H2SO4. Corros Sci 2006;48:1075–92. doi:10.1016/j.corsci.2005.05.002.

[49] Li H, Yu H, Zhou T, Yin B, Yin S, Zhang Y. Effect of Sn on the corrosion behavior of sea-water corrosion-resisting steel. Mater Des 2015;84:1–9. doi:10.1016/j.matdes.2015.06.121.

[50] Iwai Y, Yamanishi T. Thermal stability of ion-exchange Nafion N117CS membranes. Polym Degrad Stab 2009;94:679–87. doi:10.1016/j.polymdegradstab.2008.12.020.

[51] Nørgaard CF, Nielsen UG, Skou EM. Preparation of Nafion 117™-SnO2 composite membranes using an ion-exchange method. Solid State Ionics 2012;213:76–82. doi:10.1016/J.SSI.2011.10.014.

[52] Taghizadeh MT, Vatanparast M. Preparation and evaluation of Nafion/SnO2 nanocomposite for improving the chemical durability of proton exchange membranes in fuel cells. RSC Adv 2016;6. doi:10.1039/c6ra07849d.

[53] Poulsen MG, Larsen MJ, Andersen SM. Improved durability of proton exchange membrane fuel cells by introducing Sn (IV) oxide into electrodes using an ion exchange method. J Power Sources 2017;343:174–82. doi:10.1016/J.JPOWSOUR.2017.01.046.

[54] Wang K, Gasteinger HA, Markovic NM, Ross Jr PN. On the reaction pathway for methanol and carbon monoxide electrooxidation on Pt-Sn alloy versus Pt-Ru alloy surfaces. Electrochim Acta 1996;41:2587–93. doi:10.1016/0013-4686(96)00079-5.

[55] Janssen MMP, Moolhuysen J. Platinum—tin catalysts for methanol fuel cells

prepared by a novel immersion technique, by electrocodeposition and by alloying. Electrochim Acta 1976;21:861–8. doi:10.1016/0013-4686(76)85058-X.

[56] Lee SJ, Mukerjee S, Ticianelli EA, McBreen J. Electrocatalysis of CO tolerance in hydrogen oxidation reaction in PEM fuel cells. Electrochim Acta 1999;44:3283–93. doi:10.1016/S0013-4686(99)00052-3.

[57] Hinds G, Brightman E. In situ mapping of electrode potential in a PEM fuel cell. vol. 17. 2012. doi:10.1016/j.elecom.2012.01.007.

[58] Abdel Rehim SS, Sayyah SM, El Deeb MM. Corrosion of Sn in citric acid solution and the effect of some inorganic anions. Mater Chem Phys 2003;80:696–703. doi:10.1016/S0254-0584(03)00128-7.

[59] Takeno N. Atlas of Eh-pH diagrams: Intercomparison of thermodynamic databases. National Institute of Advanced Industrial Science and Technology Research Center for Deep Geological Environments; 2005.

[60] Materials FP. Freudenberg Technical Data Sheet (online) 2014. https://fuelcellcomponents.freudenberg-pm.com/products/gas-diffusion-layers (accessed July 21, 2017).

[61] Wang H, Sweikart MA, Turner JA. Stainless steel as bipolar plate material for polymer electrolyte membrane fuel cells. J Power Sources 2003;115:243–51. doi:10.1016/S0378-7753(03)00023-5.

[62] Orsi A, Kongstein OE, Hamilton PJ, Oedegaard A, Svenum IH, Cooke K. An investigation of the typical corrosion parameters used to test polymer electrolyte fuel cell bipolar plate coatings, with titanium nitride coated stainless steel as a case study. J Power Sources 2015;285. doi:10.1016/j.jpowsour.2015.03.111.

[63] Housecroft CE, Sharpe AG. Inorganic Chemistry. 2012. doi:10.1016/0022-2860(73)85197-X.

[64] Ochoa F, Williams J, Chawla N. Effects of cooling rate on the microstructure and tensile behavior of a Sn-3.5wt.%Ag solder. J Electron Mater 2003;32:1414–20.

[65] Griffiths DJ, Inglefield C. Introduction to Electrodynamics. vol. 73. 2005. doi:10.1119/1.4766311.